LANGMUIR

Interface-Rich Materials and Assemblies

Chiral Microneedles from an achiral Bis(BODIPY): Spontaneous Mirror Symmetry Breaking Leading to a Promising Photoluminescent Organic Material

Leire Gartzia-Rivero, Cesar Ray Leiva, Esther M. Sánchez-Carnerero, Jorge Bañuelos, Florencio Moreno, Beatriz L. Maroto, Inmaculada García-Moreno, Lourdes Infantes, Bianchi Mendez, Iñigo Lopez-Arbeloa, and Santiago de la Moya

Langmuir, **Just Accepted Manuscript** • DOI: 10.1021/acs.langmuir.9b00409 • Publication Date (Web): 20 Mar 2019

Chiral Microneedles from an achiral Bis(BODIPY): Spontaneous Mirror Symmetry Breaking Leading to a Promising Photoluminescent Organic Material.

Leire Gartzia-Rivero,[†] *César Ray Leiva,*[‡] *Esther M. Sánchez-Carnerero,*[∥] *Jorge Bañuelos,**[,†] *Florencio Moreno,*[‡] *Beatriz L. Maroto,*[‡] *Inmaculada García-Moreno,*[§] *Lourdes Infantes,*[¥] *Bianchi Mendez,*[⊥] *Iñigo López-Arbeloa,*[†] *and Santiago de la Moya**[,‡]

[†]Dpto. Química Física, Universidad del País Vasco (UPV/EHU), 644, 48080 Bilbao, Spain.

[‡]Dpto. Química Orgánica, Universidad Complutense de Madrid, Ciudad Universitaria s/n, 28040 Madrid, Spain.

[∥]Dpt. of Chemistry and RECETOX, Masaryk University, Kamenice 5, 62500 Brno, Czech Republic.

[§]Dpto. de Sistemas de Baja Dimensionalidad, Superficies y Materia Condensada, Instituto de Química Física Rocasolano, CSIC, Serrano 119, 28006 Madrid, Spain.

[¥]Dpto. de Cristalografía y Biología Estructural, Instituto de Química Física Rocasolano, CSIC, Serrano 119, 28006 Madrid, Spain.

[⊥]Dpto. de Física de Materiales, Universidad Complutense de Madrid, Ciudad Universitaria s/n, 28040 Madrid, Spain.

ABSTRACT. Supramolecular self-assembly of a highly flexible and achiral *meso* bis(BODIPY) dye straightforwardly yields fluorescent microfibers exhibiting an intriguing anisotropic photonic behavior. This performance includes the generation of chiroptical activity by means of spontaneous mirror symmetry breaking (SMSB). Repetition of a number of self-assembly experiments demonstrates that the involved SMSB is not stochastic but quasi deterministic in the direction of the induced chiral asymmetry. The origin of these intriguing (chiro)photonic properties is revealed by fluorescent microspectroscopy studies of individual micrometric objects, combined with X-ray diffraction elucidation of microcrystals. Such a study demonstrates that J-like excitonic coupling between bis(BODIPY) units plays a fundamental role in their supramolecular organization, leading to axial chirality. Interestingly, the photonic behavior of the obtained fibers is ruled by inherent non-radiative pathways from the involved push-pull chromophores, and mainly by the complex excitonic interactions induced by their anisotropic supramolecular organization.

INTRODUCTION

Nanostructured materials are nowadays essential scaffolds in several ongoing research projects, playing a fundamental role in the development of advanced (bio)materials for challenging (bio)technological applications. There is a vast assortment of nanostructured materials with different properties and chemical composition.[1] Currently, photonic nanomaterials are being successfully applied in innovative and socially demanded fields such as energy and biomedicine. In this regard, the development of highly-efficient active materials for energy conversion in solar cells and batteries,[2,3] as well as the design of multifunctional fluorescent nanoparticles combining highly-specific bio-sensing or bio-imaging capabilities (diagnosis) and controlled drug delivery or

singlet-oxygen photogeneration (therapy), are in the spotlight.[4-6] Among the most successful and recent approaches to achieve a proper organization at the nanometric scale, the self-assembly of organic molecules by weak noncovalent interactions is a widespread strategy to design well-defined nanostructured materials with desirable physical and chemical properties.[7-9] Such a supramolecular organization is extensively exploited by Nature to form complex biological structures, inspiring the generation of artificial systems with tailored functions.[10] Over recent years, self-assembly has brought notorious advantages in the bottom-up approach, to design highly emissive multichromophoric nanostructures[11-13] for optoelectronics[14,15], non-linear optics,[16] chirality-based applications,[17-20] or (bio)medicine[21,22]. The main advantage of these materials is their "soft" organic nature allowing wide structural diversity, as well as easy tunability of key properties, including biocompatibility.

This renewed interest in the supramolecular self-assembly of organic molecules is also supported by the intriguing photophysical processes, which can be promoted at such organization level. Indeed, to unravel and explain the peculiar excited-state dynamics occurring at the condensed phase, the commonly accepted Kasha´s exciton model (based on point-dipole approximation) has been reformulated and extended to understand challenging dipolar coupling (involving very-close neighbor molecules) existing in the mentioned phase. Thus, in fact, the widely spread concept of J-aggregation has been furnished with the term pseudo-J, or J-coupled dimers, to account for certain aggregates formed upon excitation in condensed phase.[23] Furthermore, owing to workable short-range charge-transfer interactions in closely stacked aggregates, new aggregate types have been defined, such as the HH, Hj and jH ones (with low emission probability), or the JJ and Jh ones (with high emission probability).[24] All these facts show that studying the origin of the intriguing photophysics exhibited by supramolecular systems is not an easy task. However,

knowledge in this matter is required in order to advance in the control of their interesting photonic properties. To this aim, molecular organic dyes are privileged systems, since their workable chemistry[25] allows the modulation of their assembly capability to give place to different supramolecular architectures (morphologies) exhibiting also differential photonic behaviors.

For all these reasons, it is not surprising that the popular BODIPY (boron dipyrromethene) dyes are being actively tested as luminophores in the solid state.[26-29] These dyes outstand by their excellent stability and photophysical signatures,[30] as well as by their purely-organic chromophoric core (the involved dipyrrin backbone), which is ready available to a multitude of well-known and workable organic transformations,[31,32] directed to finely design the final properties of the dye and the subsequent self-assembled material.[33,34] Herein we describe the ability of an achiral *meso* (*R*,*S*)-bis(BODIPY) (**1**) to spontaneously organize at the nanoscale via noncovalent interactions leading to luminescent microparticles (Figure 1). Such a molecular dye features two BODIPY moieties, which are linked together by their dipyrrin α-positions through the nitrogen atoms of a highly flexible diamine bridge based on achiral (*R*,*S*)-1,2-diphenylethane-1,2-diamine (**1** in Figure 1). The preparation of **1** and its fluorescent signatures in solution have been previously reported, together with those of its chiral (*R*,*R*) and (*S*,*S*) stereoisomers.[35] Besides, a challenging chiroptical behavior for these chiral stereoisomers when absorbing or emitting circularly polarized light in solution was reported.[36] It was then demonstrated that the chiroptical behavior is owing to the formation of a staggered helical conformation with a preferred configuration for its chiral axis, due to asymmetric induction.[35,36] Surprisingly, we have now found that only the *meso* stereoisomer is able to self-assemble straightforwardly (by simply solvent evaporation), yielding fluorescent micrometric needles with anisotropic response, including chiroptical activity (optical rotation and electronic circular dichroism) thanks to spontaneous mirror symmetry breaking (SMSB). All these properties,

as well as the demonstrated forces driving the self-assembly process, make the obtained material a promising photonic organic material of supramolecular nature inspiring the tailor-made preparation of similar materials with improved and controlled properties.

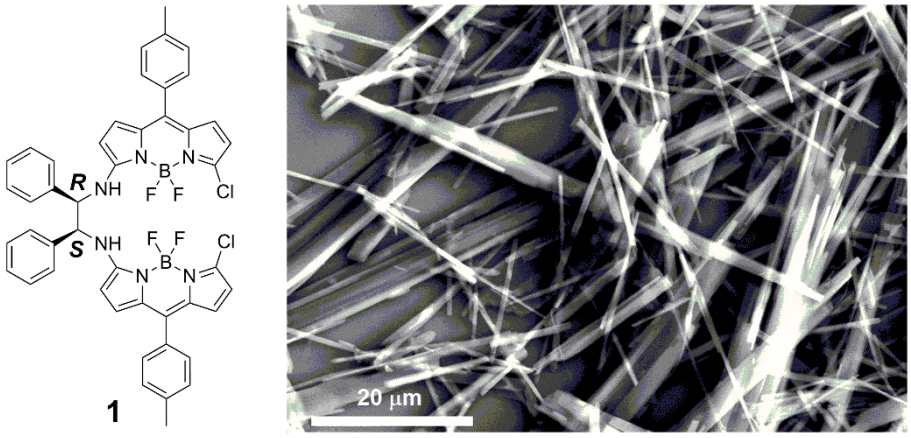

Figure 1. Chemical structure of *meso* bis(BODIPY) **1** and SEM image of the nanostructured material formed after its supramolecular assembly.

EXPERIMENTAL AND THEORETICAL METHODS

Synthesis and microstructure formation. Known *meso* bis(BODIPY) **1** was synthesized according to the described procedure and the corresponding details and characterization data reported elsewhere by us.[35] Different to that occurring with the corresponding chiral (*R*,*R*) and (*S*,*S*) stereoisomers, as well as with their racemic mixture, microstructures of *meso* **1**, as nanostructured micrometric needles (see Figure 1), were spontaneously obtained by dissolving **1** in a proper organic solvent, and then increasing its concentration in the solution by simple solvent evaporation. Common organic solvents with good capability to dissolve **1** (e.g., chloroform, 1,2-dichloroethane, or methylene chloride), as well as mixtures of them, exhibit similar capabilities

for self-assembly generating microsized needles. In order to study morphology reproducibility, we selected chloroform as the solvent, due to its higher capability to dissolve **1**. In this solvent, the formation of crystalline microstructures was proven as fully reproducible and similar morphologies and sizes were attained in different testing experiments, by using dye-concentration around 10^{-3} M in the starting solution to be casted. Spontaneous self-assembly was also proven at lower dye concentrations (below 10^{-4} M), yielding less ripened assemblies with fibrillar morphology. These morphologies were assessed with a Leica 440 scanning electron microscope operating at 15 keV.

Photophysical Properties. Absorption spectra were registered in a Varian spectrophotometer (model Cary 4E), while fluorescence steady-state spectra were recorded in an Edinburgh Instruments spectrofluorimeter (model FLSP 920). Emission spectra were corrected from the monochromators wavelength dependence, lamp profile and photomultiplier sensitivity. Absolute photoluminescence of microcrystals was recorded by means of an integrating sphere coupled to the aforementioned spectrofluorimeter.

Exciton theory calculations. The dipolar coupling of closest neighbor molecules in the molecular assembly were calculated applying Kasha's exciton theory with a simple point-dipole-approximation.[37] This model describes the resonance splitting of the excited-state energy levels for the chromophoric units (monomers) participating in a specific exciton system. In the case of systems involving parallel, but slightly slipped, transition dipoles (our case of study; see later), the exciton band splitting ε is given by Equation 1, where $|\mathbf{M}|^2$ is the transition-dipole moment for the singlet-singlet transition in the monomer, $\boldsymbol{r_{uv}}$ is the center-to-center distance between the two involved monomers (u and v), and θ is the angle between the polarization axis of a monomer and the line connecting the centers of masses of the involved monomers. The squared-matrix element

of a transition dipole moment ($|\mathbf{M}|^2$) can be expressed through the oscillator strength (f) of the corresponding transition and the light cyclic-frequency, Ω (Equation 2).

$$\Delta\varepsilon = \frac{2|M|^2}{r_{uv}^3}\left(1 - 3cos^2\theta\right) \qquad \text{(Eq. 1)}$$

$$|\mathbf{M}|^2 = \frac{e^2\hbar\, f}{2\, m_e\, \Omega} \qquad \text{(Eq. 2)}$$

Fluorescence Microspectroscopy Fluorescence images and spectroscopy of **1** assemblies at different stages of organization were recorded with an optical inverted microscope with epi configuration (Olympus BX51) equipped with a colour CCD (DP72). Sample excitation and emission was set by 470/70 band-pass and 515 nm long-pass filters (Chroma), respectively. For polarized emission images, a polarizer (U-AN-360-3) was inserted before the detection path (CCD camera) and subsequently aligned, parallel or perpendicular, to the direction of the long axis of the microfiber. Fluorescence spectra of fibers were recorded by fiber-coupling the aforementioned Olympus microscope to an Edinburgh-Instruments spectrofluorimeter (model FLSP 920).

For the microspectroscopic characterization of individual objects, we used a time-resolved fluorescence confocal microscope (Picoquant Microtime 200) with a 470 nm pulsed laser diode as the excitation source, yielding 70 ps pulses at 20 MHz repetition rate (LDH-P-C-470), whose polarization was changed to circularly polarized by a lambda/4 (Thorlabs, model WPQ05M-488). The power of the laser beam was adjusted with a neutral density wheel to around 0.1 mW at the entrance port of the microscope. Such beam was directed into the oil-immersion objective (Olympus, 1.3 N.A., 100, oil immersion) of an inverted microscope (Olympus IX70) by using a dichroic beam splitter (490DCXR, Chroma). The fluorescence signal was collected by the same objective, filtered with a 500 nm long-pass filter (Chroma), and focused (via a 50 mm pinhole)

onto an avalanche photodiode detector (Micro- Photon-Devices MPD-APD), using the method of time-correlated single photon counting (TCSPC), with a FWHM photon timing resolution better than 100 ps.

Spectroscopy was performed by directing the emission beam after the pinhole to an exit port, where a spectrograph (model Shamrock 300 mm), coupled to a CCD camera (Newton EMCCD 1600 _ 200, Andor), was mounted. FLIM results were obtained using the Symphotime fitting software, which performs a multiexponential fitting (one, two, or three exponentials depending on the sample) at each pixel.

Chiroptics. Optical rotations were recorded in a Perkin-Elmer polarimeter (model 241) from needles of **1** dispersed in chloroform (ca. 10^{-4} M). Electronic circular dichroism (ECD spectra) from such dispersions were recorded in a Jasco spectropolarimeter (model J-715) using standard quartz cells of 1-cm optical-path length.

X-ray diffraction. Single microcrystals suitable for X-ray data collection were obtained by concentrating a solution of **1** in 1,2-dichloroethane by slow solvent evaporation. 1,2-Dichloroethane was selected as the solvent due to its high vapor pressure allowing slow evaporation to grow proper crystals. A single crystal was selected, cooled at 120 K using an Oxford Cryostream device, and collected on a Bruker APEX-II CCD diffractometer. Using Olex2,[38] the structure was solved with the ShelXS[39] structure solution program, and refined with the ShelXL[40] package using Least Squares minimization. The obtained crystal structure reveals a layered structure, and the presence of disordered solvent molecules filling voids generated in the interfaces between consecutive layers along the c axis. CCDC 1851647 contains the supplementary

crystallographic data for **1**. These data can be obtained free of charge from The Cambridge Crystallographic Data Centre via www.ccdc.cam.ac.uk/getstructures.

RESULTS AND DISCUSSION

The excited state dynamics of flexible *meso* bis(BODIPY) **1** in solution is rather complex, as it also occurs for its (*R*,*R*) and (*S*,*S*) stereoisomers.[41] Thus, the electron-donating amino group and the electron-withdrawing chlorine, located at the opposite α-positions of the dypirrin, endow push-pull behavior to the chromophore and induce an intramolecular charge transfer (ICT). Besides, the unconstrained 8-tolyl group promotes a non-radiative deactivation pathway related with its free motion.[41] As a result, the fluorescence response is limited to just 10%, with decay curves analyzed as biexponentials with fast lifetimes (τ_1 = 1.05 ns (67%) and τ_2 = 0.24 ns (33%) in chloroform). On the other hand, among all the available stereoisomers, only the optically inactive one (**1**) is able to spontaneously render luminescent molecular assemblies, featuring needles with lengths of around tens to less than a hundred micrometers (Figure 1). The reason why **1** is able to self-assemble, but its chiral stereoisomers (or their racemic mixture) are not, could be ascribed to key differential spatial geometries (note diastereoisomerism), inferring disparate physical and chemical properties. Thus, diastereoisomerism may have dramatic effects on the solubility properties, which can directly affect the critical concentration needed to aggregate. In fact, the significant permanent dipole mismatch of **1** with regard to its chiral stereoisomers in solution (12.5 Debye for **1** *vs*. 7.5 Debye for the chiral stereoisomers in chloroform; see Figure S1 in Supporting Information), due to differential molecular geometries (pleated in **1** *vs*. helical in the enantiomers)[35] can lead to key different interactions. This unexpected, intriguing and specific capability of achiral **1** to self-aggregate prompted us to explore this phenomenon by means of fluorescence microspectroscopy and X-ray diffraction.

Fluorescence microspectroscopy. Figure 2 displays the fluorescence images of the two different microstructures obtained from two differently-concentrated solutions of **1** in chloroform, as described in the Experimental Section (Figure 2a, lower concentration; Figure 2c, higher concentration). Fine analysis of the images of such micro-objects reveals two clearly discernible fluorescent morphologies displaying green-yellow emission (an even red, depending on the agglomeration of the material; Figure S2 and S3 in Supporting Information), which is located preferably at the periphery of the particles for the largest ones (Figure 2c). The photoluminescence of these microcrystals decreases with regard to that obtained for **1** in solution (from 10% to 1% after the assembly), as expected in condensed phase (higher likelihood for intermolecular quenching, exciton trapping, inner filter effects, scattering, and so on),[42,43] but it is high enough as to track it easily by means of fluorescence microscopy. The observation of different micrometric morphologies could be modulated by adjusting the concentration of **1** in the chloroform solution used for the casting process (Figure 2, and Figure S3 in Supporting Information). Overall, large micro-sized needles are obtained (Figure 1 and Figure 2c), which might result from a ripening-like mechanism (e.g., the well-known Ostwald mechanism that takes place in most of the processes involving formation of nanostructures by aggregation of molecules in solution).[44] Thus, after multiple dissolution/re-aggregation steps, the initially formed nano-aggregates may grow further leading to final larger crystalline microstructures. Nonetheless, from low-concentrated enough solutions of **1**, fibrillar architectures that grow showing a dendritic fashion at the edges of the fibers, are also visualized (Figure 2a, and Figure S3 in Supporting Information). These results seem to indicate that **1** molecules self-aggregate initially forming simple wires, which, in a second stage, roll upon themselves into thicker twisted, rope-like, ripened fibers (Figure 2a).

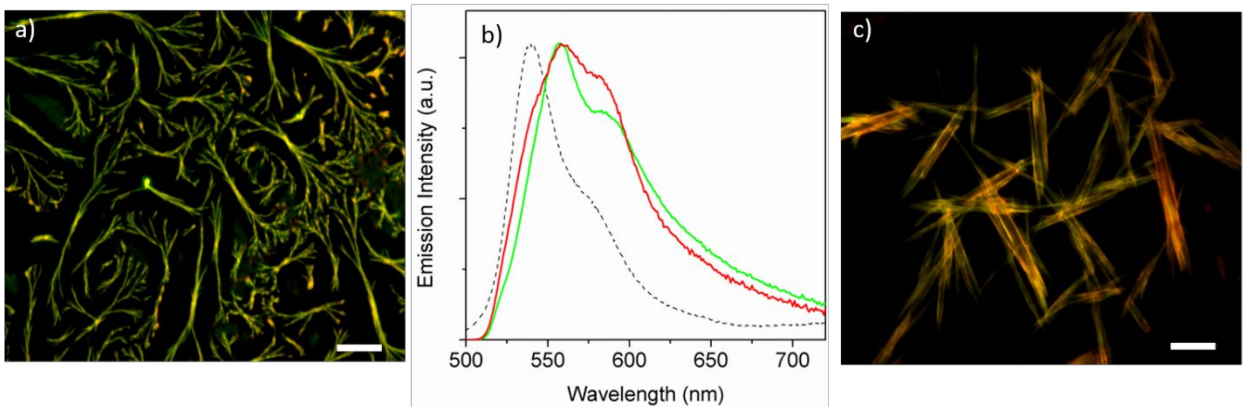

Figure 2. Fluorescence images of the two different morphologies observed for **1** (twisted fibers, from low-concentrated solutions (a) vs. needles, from high-concentrated solutions (c), 20-µm scale-bar), as well as their emission spectra (b; green spectrum for the twisted fibers, red spectrum for the needles). The emission spectrum from non-aggregated **1** in diluted solution is also included for comparison (b; dotted spectrum). Additional fluorescence images showing different stages in the self-assembly process are shown in Figure S3 in Supporting Information.

The fluorescence spectra recorded from the observed **1** micro-objects (Figure 2b) show in all cases maximum emission wavelength red-shifted with respect to that recorded from **1** in diluted solution. Such a bathochromic shift was expected due to the higher probability of re-emission/re-absorption phenomena because of the high density of chromophores existing in the solid state. On the other hand, the spectrum from twisted fibers (green spectrum in Figure 2b) shows a clear shoulder at lower energies (ca. 585 nm) with regard to the maximum emission wavelength (555 nm). This shoulder becomes more predominant in the needles (red spectrum in Figure 2b). Such broadening and red-shifting of the emission spectra of the assemblies cannot be assigned just to inner filter effects, but most probably pinpoint the presence of excitonic couplings between adjacent dye

molecules in the ensemble.[45] In fact, the absorption spectrum in the needles (see later in Figure 4) also shows a clear broadening (mainly at the long-wavelength tail) with regard to that recorded in solution.[35] These spectral signatures are characteristic of emissive J-like aggregates, which entail head-to-tail interactions between the transition dipole-moments of the involved dye molecules. However, we cannot exclude the presence of excimers as a result of π–π stacking in the excited state (in closely packed aggregates subtle changes in the geometrical arrangement can lead to differential excimer-formation capability),[12,24] since it also provides red-shifted emission patterns, albeit usually with lower fluorescence-deactivation probability than that provided by J-like aggregation.[23]

To avoid artefacts, such as inner filter effects, spectroscopy of individual objects was performed by confocal fluorescence microscopy, affording spatial, spectral and temporal resolution. Two objects, representative of each one of the recorded morphologies for **1**, were studied: (*i*) a less concentrated and braided-rope assembly with the enrolling simpler wires clearly detected at its ends (Figure 3a, in line with assemblies shown in Figure 2a); (*ii*) a densely packed and concentrated microcrystal (Figure 3c, in line with assemblies shown in Figure 2c). On the one hand, for the former object (*i*), time-resolved confocal FLIM (Fluorescence Lifetime Imaging Microscopy) image reveals a heterogeneous fluorescence lifetime distribution along the longitudinal axis of the particle (Figure 3a), from an average lifetime of ca. 0.7 ns at the edges (rolled wires in red-color code) to a shorter average lifetime of ca. 0.2 ns at the central part of the object (green to blue color- code, in Figure 3a), being the latter the main component of the whole emission-decay curve. The corresponding fluorescence spectra are also different for each monitored region of the object (see colored rectangles in Figure 3a and corresponding spectra in Figure 3b). Thus, at the fiber ends (see Figure 3a) the fluorescence profile is dominated by the

characteristic short-wavelength emission from individual **1** molecules (longer lifetimes), whereas the characteristic red-shifted emission from **1** aggregates prevails at the center of the particle (faster lifetimes). Therefore, the higher density of **1** molecules in the central region of the object favors excitonic interactions. On the other hand, the lifetime distribution of the densely packed microneedles (*ii*) is also heterogeneous along the object (Figure 3c), but with a narrower lifetime distribution and shorter values (ranging from ca. 0.35 ns to 0.15 ns). Besides, the contribution of the aggregates to the fluorescence profile is clearer, rendering a prevailing red-shifted emission (Figure 3b, dotted-line spectrum). Such a lifetime distribution through this object supports its fluorescence profile: darker in the center; brighter in the periphery (Figure 2, and Figure S4 in Supporting Information). Such a phenomenon is the consequence of a higher concentration of fluorescence quenchers (less emissive aggregates) at the center of the microparticles and likely energy migration towards the particle periphery.

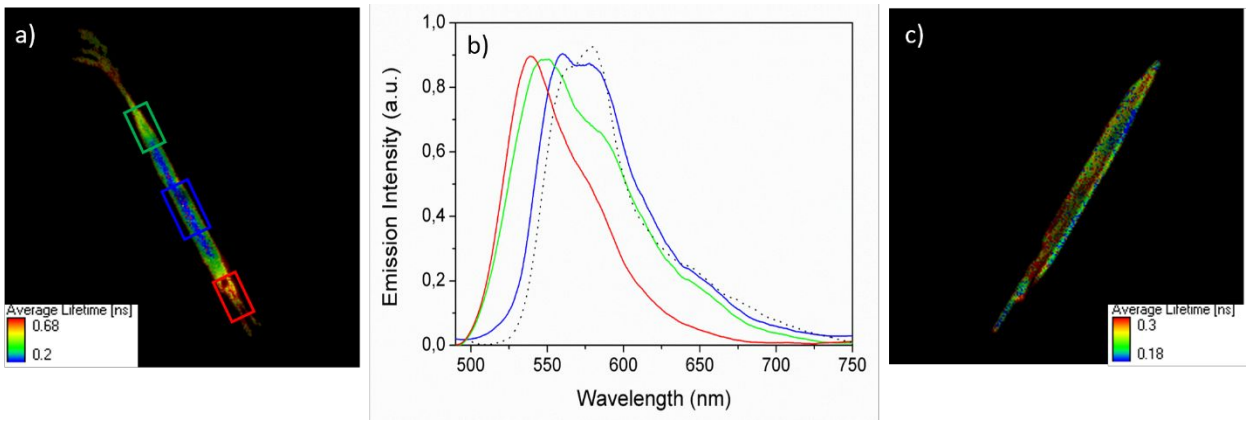

Figure 3. Time-resolved confocal FLIM images (30 x 30 μm; λ_{exc} = 470 nm, λ_{em} > 500 nm) of representative **1** objects (a: twisted fibers and c: needles, with color-code representing average decay lifetimes). Fluorescence spectra collected from different areas of the fiber-like object (b,

note color-code connecting spectra and areas highlighted with rectangles) and from the densely-packed needle-like object (b, dotted line), almost invariable along the needle (c).

Molecular packing and excitonic coupling. To unravel the driving excitonic coupling guiding the orientation and the self-assembly of **1** molecules, elucidation of the molecular packing was carried out from a single microcrystal by X-ray diffraction (Figure 4). The molecular packing reveals that, along the a-axis (Figure 4b), neighbor molecules are disposed close (R = 7.2 Å) being their respective transition-dipole moments parallel (dihedral angle between chromophoric transition moments, α, ca. 0.0°), but slightly slipped to each other (angle between the line connecting the center of masses of the dipyrrins and the chromophoric transition-dipole moment, θ, ca. 28.7°). According to Kasha's exciton theory (point-dipole approximation),[37] such tilted geometry envisages an intermolecular head-to-tail excitonic coupling (slipped angle lower than the magic angle, 54.7°, considered as the frontier between H and J aggregation), enabling a J-aggregation with a Davydov splitting of -509 cm^{-1} (Figure 4b, and Figure S5 in Supporting Information). This excitonic interaction entails a red-shifted transition (14.1 nm from the absorption maximum), which is in agreement with the broadening detected in the red edge of the absorption spectra of **1** (Figure 4d). Therefore, **1** is prone to self-assemble adopting a J-type geometry, explaining also the photonics of the detected **1** assemblies (e.g., red-shift in the emission spectra, see Figures 2 and 3). Furthermore, **1** molecules also stack along the b-axis but, in this case, the main driving forces correspond to π–π interactions involving two close pendant phenyls of neighboring diamine-based bridges, as well as specific intermolecular interactions involving pendant-phenyl hydrogens and dipyrrin electronic clouds (H$\cdots\pi$ interactions with distance ca. 3

Å; see Figure 4c). Finally, these two-dimensional structures stack together along the c-axis by means of hydrophobic interactions (the BODIPY scaffold is well known for its hydrophobic character),[30-32] leading to three-dimensional microstructures. In such a supramolecular organization, with high density of dichromophoric **1** molecules, further excitonic interactions like π–π stacking or excimers should not be discarded. As a result, the recorded fluorescence spectra of the detected micro-objects covers the contribution of individual dipyrrin chromophores and coupled entities involving such chromophores.

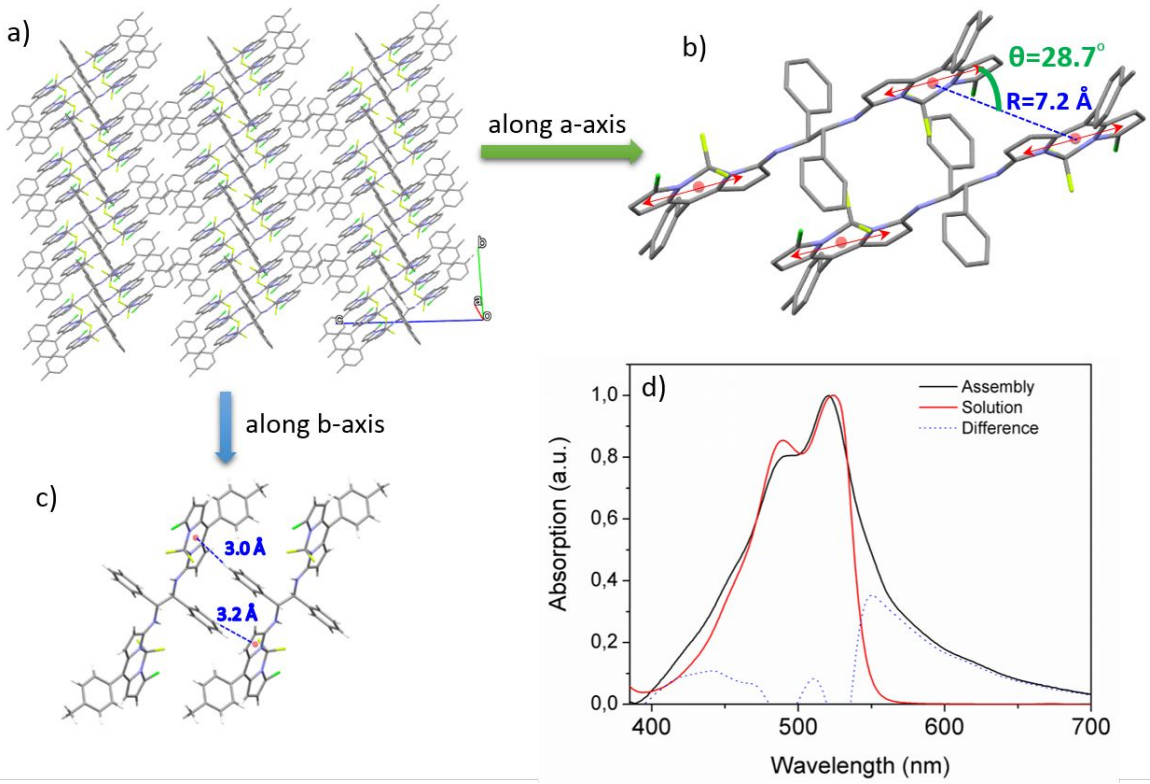

Figure 4. X-Ray resolved crystalline packing of **1** (a), detailed packing along the a- and b-axis (b and c, respectively) and absorption spectra of **1** (d; red in solution, black in solid state, and blue-dotted for the corresponding subtraction spectrum, the later as a tool for detecting possible absorption signatures from aggregates). Distances between transition-dipole moments, and

corresponding θ angles, for key couplings involving the nearest units are also given (see b). Red double-head arrows indicate the emission dipoles disposed along the longitudinal axis of the dipyrrin chromophores (see b). The unit cell is triclinic (space group P-1; a = 7.16 Å, b = 9.43 Å and c = 19.04 Å).

Anisotropy and chiroptics. The supramolecular organization of **1** should entail an anisotropic photonic behavior due to the preferential orientation of the molecules within the microfiber. This assumption was confirmed by the detection of on/off switching of the needle emission by passing such an emission through a polarizer disposed parallel (fluorescence on) or orthogonal (fluorescence off) to the longitudinal axis of the microcrystal (Figure 5). This result supports that the transition-dipole moments are preferably placed parallel to this axis. Additional analysis of the anisotropic response shows that the brighter and red-shifted peripheral areas of the particles are less polarized (Figure 5), anticipating that the degree of order is notoriously reduced in these regions. This fact could also point towards the presence of energy migration processes, from the center to the edges of the microcrystal (Figure S4 in the Supporting Information), which would be mediated by less energetic species acting as energy traps and depolarizing the output light.

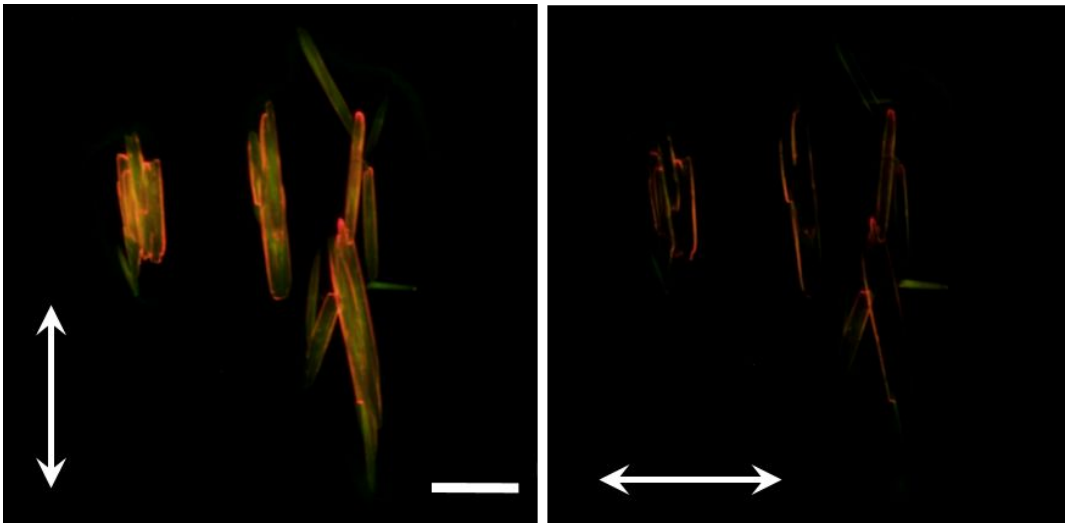

Figure 5. Fluorescence images (λ_{exc} = 470 nm, λ_{em} > 515 nm, by wide-field microscopy) of a set of **1** needles with parallel and orthogonal polarizations, respectively, in the collected emissions (arrows indicate the direction of the emitted polarized light; 20-µm scale-bar).

Another remarkable anisotropic photonic behavior of the **1** needles is the existence of chiroptical activity (see later), taking into account that individual **1** molecules are achiral (*meso*). Accordingly, such individual molecules, which were demonstrated to adopt a bended folder conformation in solution, exhibit silent ECD (Figure 6).[35] However, owing to the packing energy in the solid state, **1** molecules flip to a helical (chiral) conformation, involving a staggered disposition of their dipyrrin units and pendant diamine-bridge phenyls (Figure 6). This helical conformation is similar to that exhibited by the chiral stereoisomers of **1** in solution, where the helical configuration (*M* or *P*) is asymmetrically induced by the own chirality (*R,R or S,S* center-chirality) of the corresponding stereoisomer.[35] However, this asymmetric induction in the helical chirality is not possible in *meso* **1**. Therefore, the observed optical activity for **1** needles must be originated by the interesting phenomenon known as spontaneous mirror symmetry breaking (SMSB),[46-48] working during the self-aggregation of **1** molecules disposed in the said helical configuration.

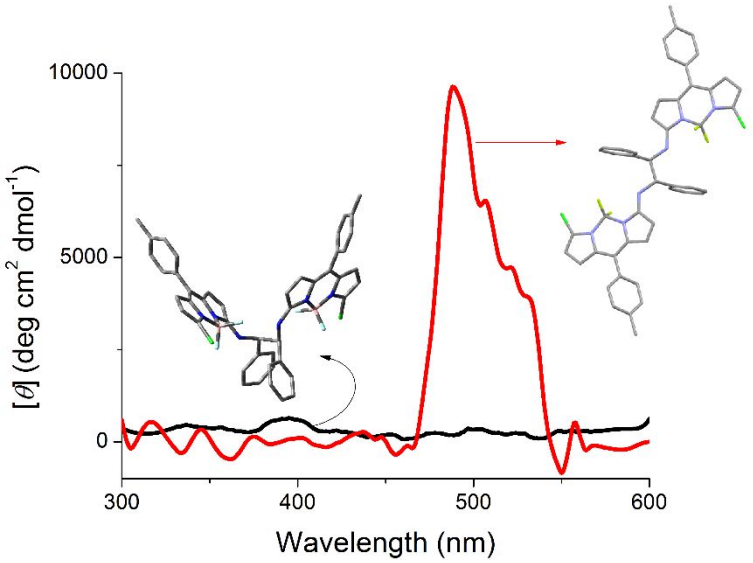

Figure 6. Representative ECD spectra of individual (black) and aggregated (red; smoothed) **1** molecules in chloroform (dye concentration $6.9 \cdot 10^{-6}$ M and $1.4 \cdot 10^{-4}$ M, respectively). The corresponding molecular geometries (pleated in solution *vs*. helically chiral in the aggregates) are also included. Note the helically chiral molecules in the assembly are also interacting with neighbor molecules by complex excitonic processes, including J-type interaction (see Figure 4), which would explain the lack of bisignalization for the aggregate ECD signal. For additional examples of ECD spectra from aggregated **1** in chloroform (needles dispersion) at different concentrations, see Figure S6 in Supporting Information.

The observed chiroptical activity consists in the detection of a weak, but statistically reproducible, visible ECD signal from **1** needles dispersed in chloroform (see representative ECD spectra in Figure 6, and Figure S6 in Supporting Information), as well as in the detection of optical rotation for such dispersions. Repetition of a large number (ca. 100) of aggregation experiments, followed by ECD and optical-rotation recording, all of them under identical experimental conditions, was

carried out. Interestingly, the results of these measurements show that the required SMSB during the aggregation is not stochastic for the signs of both ECD and optical rotation. Thus, ca. half (48%) of the studied needles dispersions in chloroform ($5.94 \cdot 10^{-5}$ M in terms of **1** molecules) gave place to silent or positive spectra (36% and 16% of the cases, respectively, in terms of molar ellipticity, [θ]; e.g., see Figure 6). Remarkably, clearly negative ECD spectra (note the noise in these ECD spectra) were not detected in any case. In the other half of the studied cases, the output signal saturation (due to light dispersion by the aggregates) was observed. This result shows that the involved SMSB is not stochastic but quasi deterministic in the direction of the induced chiral asymmetry. This finding is also supported by the conducted optical-rotation study of the obtained needles dispersions. Thus, it was found that the specific rotation, $[\alpha]_D^{20}$, of the dispersions varies rapidly over time, but most of the obtained values (ca. 90%) were negative, ranging from -6.1 to -110.4 $deg \cdot dm^{-1} \cdot cm^3 \cdot g^{-1}$ (c = 0.0054 g/100 ml). These results suggest the existence of a dynamic aggregation/disaggregation process in such dispersions. The process would involve helically-chiral molecules with a preferred helical configuration (non-stochastic SMSB) in the aggregated state, and individual achiral molecules in solution (aggregated and disaggregated **1**, respectively). It must be noted here that non-stochastic SMSB is not striking, since a characteristic of this phenomenon is that a very weak chiral effect (non-detected) can efficiently select one of the two degenerated chiral branches.[49-51]

CONCLUSIONS

The significant capability of an achiral (*meso*) bis(BODIPY) dye to aggregate generating a (chiro)photoactive nanostructured material is reported and studied. Such a nanostructured material consists of needles-like fluorescent micro-objects, formed by the supramolecular organization of a starting aggregating template: a synthetically accessible bis(BODIPY) unit able to predispose in

a helically chiral conformation to self-aggregate. The main driving force for the self-assembly of such a template is the formation of intramolecular J-aggregates with red-shifted emission. Afterwards, such aggregates wrapped each other leading to densely packed micro-architectures, owing to hydrophobic and intermolecular H···π interactions, the later involving pendant-phenyl hydrogens and dipyrrin moieties (π-system). The involved supramolecular organization provides a well-defined organization of the dye molecules, leading to an interesting anisotropic fluorescent material emitting polarized light, and exhibiting chiroptical activity due to spontaneous mirror symmetry breaking. Further work is in progress to modulate morphology, chirality and photophysics in this readily-accessible nanostructured organic material, by studying the possible synergic influence of different variables (concentration, solvent, temperature, presence of chiral inducers) in the aggregation process.

ASSOCIATED CONTENT

Supporting Information. The following files are available free of charge: computed both molecular permanent dipolar moments and electrostatic potential surfaces for *meso* **1** and its chiral (*R*,*R*) stereoisomer (Figure S1), transmission and fluorescence images of **1** micro-objects (Figure S2, S3 and S4), calculated Davydov splitting for possible dipole couplings in the assembly (Figure S5), and ECD spectra recorded from **1** in chloroform at different concentrations (Figure S6).

AUTHOR INFORMATION

Corresponding Author

*E-mail: jorge.banuelos@ehu.es, santmoya@ucm.es

Author Contributions

The manuscript was written through contributions of all authors. All authors have given approval to the final version of the manuscript.

ACKNOWLEDGMENTS

We gratefully acknowledge the Spanish Ministerio de Economia y Competitividad for financial support (projects MAT2017-83856-C3-1-P, 2-P and 3-P). We also acknowledge Gobierno Vasco for financial support (project IT912-16).

REFERENCES

(1) Yin, Y; Talapin, D. The chemistry of functional nanomaterials. *Chem. Soc. Rev.* **2013**, *42*, 2484-2487.

(2) Sun, Y.; Liu, N; Cui, Y. Promises and challenges of nanomaterials for lithium-based rechargeable batteries. *Nat. Energy* **2016**, *1*, 16071.

(3) Green, M. A.; Bremmer, S. P. Energy conversion approaches and materials for high-efficiency photovoltaics. *Nat. Mater.* **2017**, *16*, 23-34.

(4) Doane, T. L.; Burda, C. The unique role of nanoparticles in nanomedicine: imaging, drug delivery and therapy. *Chem. Soc. Rev*. **2012**, *41*, 2885-2911.

(5) Biju, V. Chemical modifications and bioconjugate reactions of nanomaterials for sensing, imaging, drug delivery and therapy. *Chem. Soc. Rev*. **2014**, *43*, 744-764.

(6) Wolfbeiss, O. S. An overview of nanoparticles commonly used in fluorescent bioimaging. *Chem. Soc. Rev*. **2015**, *44*, 4743-4768.

(7) Stupp, S. I.; Palmer, L. C. Supramolecular chemistry and self-assembly in organic materials design. *Chem. Mater*. **2014**, *26*, 507−518.

(8) Würthner, F.; Saha-Möller, C. R.; Fimmel, B.; Ogi, S.; Leowanawat, P.; Schmidt, D. Perylene bisimide dye assemblies as archetype functional supramolecular materials. *Chem. Rev*. **2016**, *116*, 962-1052.

(9) Sevim, S.; Sorrenti, A.; Franco, C.; Furukawa, S.; Pané, S.; deMello, A. J.; Puigmartí-Luis, J. Self-assembled materials and supramolecular chemistry within microfluid environments: from common thermodynamic states to non-equilibrium structures. *Chem. Soc. Rev.* **2018**, *47*, 3788-3803.

(10) Boekhoven, J.; Brizard, A. M.; Stuart, M. C. A.; Florusse, L.; Raffy, G.; Del Guerzo, A.; Van Esch, J. H. Bio-inspired supramolecular materials by orthogonal self-assembly of hydrogelators and phospholipids. *Chem. Sci*. **2016**, *7*, 6021-6031.

(11) Acuna, G. P.; Möller, F. M.; Holzmesiter, P.; Beater, S.; Lalkens, B.; Tinnefeld, P. Fluorescent enhancement at docking sites of DNA-directed self-assembled nanoantennas. *Science* **2012**, *338*, 506-510.

(12) Gierschner, J.; Park, S. Y. Luminescent distyrylbenzenes: tailoring molecular structure and crystalline morphology. *J. Mater. Chem. C* **2013**, *1*, 5818-5832.

(13) Maggini, L.; Bonifazi, D. Hierarchised luminescent organic architectures: design, synthesis, self-assembly, self-organisation and functions. *Chem. Soc. Rev*. **2012**, ***41***, 211-241.

(14) Busseron, E.; Ruff, Y.; Moulin, E.; Giuseppone, N. Supramolecular self-assemblies as functional nanomaterials. *Nanoscale* **2013**, *5*, 7098-7140.

(15) Gierschner, J.; Varghese, S.; Park, S. Y. Organic single crystal lasers: a materials view. *Adv. Opt. Mater*. **2016**, *4*, 348-364.

(16) Xu, J.; Semin, S.; Niedzialek, D.; Kouwer, P. H. J.; Fron. E.; Coutino, E.; Savoini, M.; Li, Y.; Hofkens, J.; Uji-I, H.; Beljonne, D.; Rasing, T.; Rowan, A. E. Self-assembled organic microfibers for nonlinear optics. *Adv. Mater*. **2013**, *25*, 2084-2089.

(17) García, F.; Sánchez, L. Structural rules for the chiral supramolecular organization of OPE-based discotics: induction of helicity and amplification of chirality. *J. Am. Chem. Soc*. **2012**, *134*, 734-742.

(18) Wang, Y.; Xu, J.; Wang, Y.; Chen, H. Emerging chirality in nanoscience. *Chem. Soc. Rev*. **2013**, *42*, 2930-2962.

(19) Valev, V. K.; Baumberg, J. J.; Sibilia, C.; Verbiest, T. Chirality and chiroptical effects in plasmonic nanostructures: fundamentals, recent progress, and outlook. *Adv. Mater.* **2013**, *25*, 2517-2534.

(20) Han, J.; Guo, S.; Lu, H.; Liu, S.; Zhao, Q.; Huang, W. Recent progress on circularly polarized luminescent materials for organic optoelectronic devices. *Adv. Opt. Mater*. **2018**, *6*, 1800538.

(21) Sinkeldam, R. W.; Greco, N. J.; Tor. Y. Fluorescent analogs of biomolecular building blocks: design, properties and applications. *Chem. Rev*. **2010**, *110*, 2579-2619.

(22) Fateminia, S. M. A.; Wang, Z.; Goh, C. C.; Manghnnani, P. N.; Wu, W.; Mao, D.; Ng, L. G.; Zhao, Z.; Tang, B. Z.; Liu, B. Nanocrystallization: A unique approach

to yield bright organic nanocrystals for biological applications. *Adv. Mater*. **2017**, *29*, 1604100.

(23) Musser, J.; Rajendran, S. K.; Georgiu, K.; Gai, L.; Grant, R. T.; Shen, Z.; Cavazzini, M.; Ruseckas, A:, Turnbull, G. A.; Samuel, I. D. W.; Clark, J.; Lidzey, D. G. Intermolecular states in organic dye dispersions: excimers vs aggregates. *J. Mater. Chem. C* **2017**, *5*, 8380-8389.

(24) Hestand, N. J.; Spano, F. C. Molecular aggregate photophysics beyond the Kasha model: novel principles for organic materials. *Acc. Chem. Res*. **2017**, *50*, 341-350.

(25) De Moliner, F.; Kielland, N.; Lavilla, R.; Vendrell, M. Modern synthetic avenues for the preparation of functional fluorophores. *Angew. Chem. Int. Ed*. **2017**, *56*, 3758-3769.

(26) Liao, Y.; Genot, V.; Meallet-Renault, R.; Vu, Y. T.; Audibert, J.-F.; Lemaistre, J.-P.; Clavier, G.; Retailleau, P.; Pansu, R. B. Spectroscopy of BODIPYs in solid phase: crystal and nanoparticles. *Phys. Chem. Chem. Phys*. **2013**, *15*, 3186-3195.

(27) Choi, S.; Bouffard, J.; Kim, Y. Aggregation-induced emission enhancement of a meso-trifluoromethyl BODIPY via J-aggregation. *Chem. Sci*. **2014**, *5*, 751-755.

(28) Kim, S.; Bouffard, J.; Kim, Y. Tailoring the sold-state fluorescence emission of BODIPY dyes by meso substitution. *Chem. Eur. J*. **2015**, *21*, 17459-17465.

(29) Maeda, C.; Todaka, T.; Ueda, T.; Ema, T. Color-tunable solid-state fluorescence emission from carbazole-based BODIPYs. *Chem. Eur. J*. **2016**, *22*, 7508-7513.

(30) Bañuelos, J. BODIPY dye, the most versatile fluorophore ever? *Chem. Rec*. **2016**, *16*, 335-348.

(31) Boens, N.; Verbelen, B.; Dehaen, W. Postfunctionalization of the BODIPY core: synthesis and spectroscopy. *Eur. J. Org. Chem.* **2015**, 6577-6595.

(32) Lakshmi, V.; Sharma, R.; Ravikanth, M. Functionalized boron-dipyrromethenes and their applications. *Rep. Org. Chem*. **2016**, *6*, 1-24.

(33) Cherumukkil, S.; Vedhanarayanan, B.; Das, G.; Praveen, V. K.; Ajayaghosh, A. Self-assembly of BODIPY-derived extended π-systems. *Bull. Chem. Soc. Jpn*. **2018**, *91*, 100-120.

(34) Solomonov, A. V.; Marfin, Y. S.; Rumyantsev, E. V. Design and applications of dipyrrin-based fluorescent dyes and related organic luminophores: from individual compounds to supramolecular self-assembled systems. *Dyes and Pigments* **2019**, *162*, 517-542.

(35) Sánchez-Carnerero, E. M.; Moreno, F.; Maroto, B. L.; Agarrabeitia, A. R.; Bañuelos, J.; Arbeloa, T.; López-Arbeloa, I.; Ortiz, M. J., de la Moya, S. Unprecedented induced axial chirality in a molecular BODIPY dye: strongly bisignated electronic circular dichroism in the visible region. *Chem. Commun*. **2013**, *49*, 11641-11643.

(36) Ray, C.; Sánchez-Carnerero, E. M.; Moreno, F.; Maroto, B. L.; Agarrabeitia, A. R.; Ortiz, M. J.; López-Arbeloa, I.; Bañuelos, J.; Cohovi, K. D.; Lunkley, J. L.; Muller, G.; de la Moya, S. Bis(haloBODIPYs) with labile helicity: valuable simple organic molecules that enable circularly polarized luminescence. *Chem. Eur. J.* **2016**, *22*, 8805-8808.

(37) Kasha, M.; Rawls, H. R.; El-Bayoumi, M. A. The exciton model in molecular spectroscopy. *Pure Appl. Chem.* **1965**, *11*, 371-392.

(38) Dolomanov, O. V.; Bourhis, L. J.; Gildea, R. J.; Howard, J. A. K.; Puschmann, H. OLEX2: a complete structure solution refinement and analysis program. *J. Appl. Cryst*. **2009**, *42*, 339-341.

(39) Sheldrick, G. M. A short history of SHELX. *Acta Cryst*. *A* **2008**, *64*, 112–122.

(40) Sheldrick, G. M. Crystal structure refinement with SHELX. *Acta Cryst*. *C* **2015**, *71*, 3-8.

(41) Ray, C.; Bañuelos, J.; Arbeloa, T.; Maroto, B. L.; Moreno, F.; Agarrabeitia, A. R.; Ortiz, M. J.; López-Arbeloa, I.; de la Moya, S. Push-pull flexibly-bridged bis(haloBODIPYs): solvent and spacer switchable red emission. *Dalton Trans*. **2016**, *45*, 11839-11848.

(42) Hinton, D. A.; Ng, J. D.; Sun, J.; Lee, S.; Saikin, S. K.; Logsdon, J.; White, D. S.; Marquard, A. N.; Cavell, A. C.; Krasecki, V. K.; Knapper, K. A.; Lupo, K. M.; Wasieleswski, M. R.; Aspuru-Guzik, A.; Biteen, J. S.; Gopalan, P.; Goldsmith, R. H. mapping forbidden emission to structure in self-assembled organic nanoparticles. *J. Am. Chem. Soc.* **2018**, *140*, 15827-15841.

(43) Rodriguez, H. B.; Mirenda, M.; Lagorio, M. G.; San Román, E. Photophysics at unusually high dye concentrations. *Acc. Chem. Res*. **2019**, *52*, 110-118.

(44) Lilly, G. D.; Lee, J.; Sun, K.; Tang, Z.; Kim, K.-S.; Kotov, N. A. Media effect on CdTe nanowire growth: mechanism of self-assembly, Ostwald ripening, and control of NW geometry. *J. Phys. Chem. C* **2008**, *112*, 370-377.

(45) Wang, B.; Mu, G.; Lv, X.; Ma, L.; Zhuang, S.; Wang, L. Tuning electron injection/transporting properties of 9,10-diphenylanthracene based electron

transporters via optimizing the number of peripheral pyridine for highly efficient fluorescent OLEDs. *Org. Electron.* **2016**, *34*, 179-187.

(46) Hamel, P.; Haddadi, S.; Raineri, F.; Monnier, P.; Beaudoin, G.; Sagnes, I.; Levenson, A.; Yacomotti, A. M. Spontaneous mirror-symmetry breaking in coupled photonic-crystal nanolasers. *Nat. Photon*. **2015**, *9*, 311-315.

(47) Tschierske, C.; Ungar, G. Mirror symmetry breaking by chirality synchronization in liquids and liquid crystals of achiral molecules. *ChemPhysChem* **2016**, *17*, 9-26.

(48) Pavlov, V. A.; Zlotin, S. G. Homochirality, stochastic chiral reactions, spontaneous chiral ordering of achiral molecules, and similar chiral effects. Is there a physical basis for these mirror symmetry breaking phenomena? *Curr. Org. Chem*. **2018**, *22*, 2029-2054.

(49) Kondepudi, D. K., Prigogine, I.; Nelson, G: Sensitivity of branch selection in nonequilibrium systems. *Phys. Lett. A* **1985**, *111*, 29-32.

(50) Avetisov, V. A.; Kuz'min, V. V.; Anikin, S. A. Sensitivity of chemical chiral systems to weak asymmetric factors. *Chem. Phys*. **1987**, *112*, 179-187.

(51) Ribo, J. M.; Crusats, J.; El-Hachemi, Z.; Moyano, A.; Hochberg, D. Spontaneous mirror symmetry breaking in heterocatalytically coupled enantioselective replicators. *Chem. Sci*. **2017**, *8*, 763-769.

For Table of Contents Use